World Academy of Science, Engineering and Technology
International Journal of Mechanical and Mechatronics Engineering
Vol:4, No:8, 2010

Flexible Follower Response of a Translating Cam with Four Different Profiles for Rise-Dwell-Fall-Dwell motion

Jer-Rong Chang
Department of Aircraft Engineering, Air Force Institute of Technology
1, Jyulun Road, Gang-Shan Township, Kaohsiung County 820, Taiwan, ROC
Email: jerrong.chang@gmail.com

***Abstract*—**The flexible follower response of a translating cam with four different profiles for rise-dwell-fall-dwell (RDFD) motion is investigated. The cycloidal displacement motion, the modified sinusoidal acceleration motion, the modified trapezoidal acceleration motion, and the 3-4-5 polynomial motion are employed to describe the rise and the fall motions of the follower and the associated four kinds of cam profiles are studied. Since the follower flexibility is considered, the contact point of the roller and the cam is an unknown. Two geometric constraints formulated to restrain the unknown position are substituted into Hamilton's principle with Lagrange multipliers. Applying the assumed mode method, one can obtain the governing equations of motion as non-linear differential-algebraic equations. The equations are solved using Runge-Kutta method. Then, the responses of the flexible follower undergoing the four different motions are investigated in time domain and in frequency domain.

***Keywords*—**translating cam, flexible follower, rise-dwell-fall-dwell, response

I. INTRODUCTION

Pasin [1] studied a valve control mechanism of internal combustion engines. The longitudinal vibrations of the moving rod were neglected, and the rod was loaded by a variable axial force. The equation of bending vibrations of this rod was obtained using the classical bending theory and d'Alembert's principle. Then the partial differential equation with variable coefficients was reduced to a system of ordinary differential equations of second order with periodic coefficients using Galerkin method. The stability of the rod and consequently of the cam mechanism was investigated according to the parameters of speed and stroke. Yilmaz and Kocabas [2] studied the longitudinal vibrations of a follower which is the linear active component of a cam mechanism. The basic Bernoulli method was applied to solve the partial differential equation which was supplied by taking the viscous damping factor into consideration. Followers driven by high-speed, dwell-type, rotating disk cams can exhibit undesirable residual vibrations during dwell. Felszeghy [3] studied a cam with a translating roller follower. He idealized the follower structure as a single degree-of-freedom, spring-mass-dashpot, linear system. These residual vibrations were obtained with closed-form solutions to the steady-state vibrations obtained with a circular convolution integral. The steady-state vibrations, which can extend over the entire cam cycle, were periodic and continuous.

Teodorescu and Rahnejat [4] introduced a fast converging mathematical model to predict the peculiarities of the non-conforming contact between an infinitely long cylinder and a coated elastic substrate. The proposed method was then integrated into a multi-physics analysis of the valve train system of a racing type internal combustion engine. Due to relatively high loads and speeds experienced, particularly in the cam-tappet contacts, hard wear resistant coatings are used, which greatly influence the contact mechanics performance. Results indicate that the layer thickness is the determining factor in contact characteristics, which alters during the cam cycle. Therefore, for optimal performance coatings of non-uniform thickness should ideally be applied to the circumference of the cam rather than the usual coating of the tappet surface with a given thickness. Wu etc. [5] studied that a translating cam driven by an offset slider-crank mechanism has varying velocity, and the follower motion can be arbitrarily chosen for only the forward or the return stroke of the translating cam. By employing the concept of velocity instant center, the cam profile, the path of cutter, the pressure angle and the radius of curvature of the cam can be expressed parametrically, and the follower motion of the remaining stroke can be analyzed analytically. The cam profile has concave, convex and flat portions. Cveticanin [6] modeled the mechanism as a cam-follower-driveshaft system where the flexibility of the camshaft and of the follower was considered. The dynamics of cam mechanism was analyzed. The non-linear and damping properties of the system were also taken into consideration. For constant angular velocity of the cam the mechanism was modeled as a two-degree-of-freedom system. The mathematical model of the system was described with two coupled parametrically excited non-linear second-order differential equations. The stability of motion of the system has been investigated. Based on the criterion of stability the method for obtaining cam profile was developed. The conditions for stable and asymptotic stable motion of the follower were analytically determined.

Wu etc. [7] proposed a novel translating follower that has symmetrical double rollers and also demonstrated how to design such a cam mechanism. Two identical rollers are symmetrically mounted on opposite sides of the follower. The two rollers take turns to contact the cam when the cam rotates. The application of this follower can greatly reduce the pressure angle on both the rising and the falling motions of the follower. It may also reduce the induced forces. Naskar and Acharyya [8] conducted a comprehensive experimental analysis for measuring dynamic response of jerk optimized, stress optimized and size optimized cams, with advanced techniques of data acquisition and data processing. A precision manufacturing process was employed

for preparing cam surface. Results showed close matching of experimental outputs with theoretical predictions of displacement and values of follower preset. A method was suggested for specifying the causes behind deviations of predicted cam displacements from actual displacements.

In this paper, the flexible follower response of a translating cam with four different profiles for RDFD motion is investigated. The follower rod pinned with a roller which is restrained within the rotating cam groove. Since the follower flexibility is considered, the contact point of the roller and the cam is an unknown. Two geometric constraints are established to restrain the unknown contact position. They are substituted into Hamilton's principle as Lagrange multipliers. The transverse deflection of the follower is expanded with the assumed mode method in which the mode is time-dependent since the follower is driven to lengthen or shorten when the cam is rotating. The follower response with four different profiles for RDFD motion is obtained. The time histories and the FFT spectra of the flexible follower responses are investigated.

Ⅱ. DERIVATION OF GOVERNING EQUATIONS

A cam mechanism including a rigid cam with a translating roller-follower is shown in Fig. 1. The flexible follower rod is assumed to be Rayleigh beam. The follower rod has a separate part, the roller, which is pinned to the follower stem. Since the roller moves in groove, the roller maintains contact with the cam and rolls on the cam surface as the cam rotates. The rigid-body translating motion and the flexible transverse deflection are constrained by the contact constraints.

The kinetic energy and strain energy of the follower, the kinetic energy of the roller, and the work done by the constraint forces are formulated first. The follower deflections are expanded using the assumed mode method. Then, the governing equations of the flexible follower rod are derived by employing Hamilton's principle.

2.1 The kinetic energy and strain energy of the system

Using the envelopes theory to determine the cam profile, the profile coordinates (x_{1C}, y_{1C}) are derived as (refer to Fig. 1)

$$\begin{aligned} x_{1C} &= r\cos\theta - \frac{r_r Q}{\sqrt{P^2+Q^2}}, \\ y_{1C} &= r\sin\theta + (x - r\cos\theta)\frac{P}{Q}. \end{aligned} \tag{1}$$

where

$$\begin{aligned} r &= r_b + r_r + S(\theta), \\ P &= r\sin\theta - S'(\theta)\cos\theta, \\ Q &= r\cos\theta - S'(\theta)\sin\theta. \end{aligned} \tag{2}$$

in which r_b is the base-circle radius of the cam, and r_r is the roller radius.

And the coordinates of the roller center *E* are

$$\begin{aligned} x_{1E} &= r\cos\theta, \\ y_{1E} &= r\sin\theta. \end{aligned} \tag{3}$$

A rotating frame $O_1 - x_1 y_1$ fixed on the cam which rotates with a constant angular speed Ω is shown in Fig. 2. A fixed frame $O_2 - xy$ is also used and its unit coordinate vectors are denoted as $\{\mathbf{i}, \mathbf{j}\}^T$. The $O_2 x$ axis coincides with the centerline of the undeformed rod. The flexible follower undergoes a transverse deflection, $v(x,t)$. The end point *E* moves to be E' after deformation. The transverse deflection at the end point *E* are denoted as v_E, i.e., $v_E = v(l,t)$. A fixed frame $O_1 - XY$ is also used. The fixed coordinates for the points *C* and *E* are

$$\begin{aligned} X_C &= x_{1C}\sin\Omega t - y_{1C}\cos\Omega t, \\ Y_C &= x_{1C}\cos\Omega t + y_{1C}\sin\Omega t, \\ X_E &= x_{1E}\sin\Omega t - y_{1E}\cos\Omega t, \\ Y_E &= x_{1E}\cos\Omega t + y_{1E}\sin\Omega t. \end{aligned} \tag{4}$$

2.1.1 The kinetic energy and strain energy of the rod

An arbitrary point *P* on a cross-section of the follower rod is deformed to be the point P', shown in Fig. 2. The position vector $\mathbf{R}_{P'}$ can be expressed as

$$\mathbf{R}_{P'} = (x - yv_{,x})\mathbf{i} + (y + v)\mathbf{j} \tag{5}$$

where the subscript means to take partial derivative with respect to x.

The velocity of the point P' is derived as

$$\dot{\mathbf{R}}_{P'} = [\dot{x} - y\dot{v}_{,x}]\mathbf{i} + \dot{v}\mathbf{j} \tag{6}$$

where the dot symbol means to take derivative with respect to time t.

The kinetic energy T_{rod} of the rod can be expressed as

$$\begin{aligned} T_{rod} &= \frac{1}{2}\iiint_V \rho\dot{\mathbf{R}}_{P'}\cdot\dot{\mathbf{R}}_{P'}\,dV \\ &= \frac{1}{2}\int_0^{x_E}\rho A(\dot{x}^2 + \dot{v}^2)\,dx + \frac{1}{2}\int_0^{x_E}\rho I\dot{v}_{,x}^2\,dx \end{aligned} \tag{7}$$

where ρ denotes the mass density of the rod. *A* is cross-sectional area of the rod. *I* is the area moment of inertia of the rod cross-section. It is known form Eq. (7) that the kinetic energy of the rod contains the rigid-body and flexible translational and rotational energies.

Applying the strain-stress relationship of Hooke's law, one has the strain energy U_{rod} of the rod as follows,

$$U_{rod} = \frac{1}{2}\iiint_V E(-yv_{,xx})^2 dV = \frac{1}{2}\int_0^{x_E} EIv_{,xx}^2 dx \quad (8)$$

where E denotes Young's modulus of beam material.

2.1.2 The kinetic energy of the roller

The kinetic energy of the roller including the translational and rotational energies is derived as

$$\begin{aligned} T_{roller} &= \frac{1}{2} m_r \dot{\mathbf{R}}_{E'} \cdot \dot{\mathbf{R}}_{E'} + \frac{1}{2} J_r \dot{\theta}_r^2 \\ &= \frac{1}{2} m_r (\dot{X}_E{}^2 + \dot{Y}_E{}^2) \\ &\quad + \frac{1}{2}\frac{J_r}{r_r^2}[(\dot{X}_C - \dot{X}_E)^2 + (\dot{Y}_C - \dot{Y}_E)^2] \end{aligned} \quad (9)$$

where m_r and J_r are the mass and the polar mass moment of inertia of the roller, respectively.

2.1.3 Constraint equations

From the geometric relationship as shown in Fig. 2, two constraint equations for the point E are derived as

$$\Phi_1 = X_E - v_E = 0 \quad (10)$$

$$\Phi_2 = Y_E + x_E - d = 0 \quad (11)$$

It is seen that the rigid-body motion and the flexible vibration are coupled under the geometric constraints.

2.2 Assumed mode method

One end of the follower rod is restrained with a rigid cylinder and the other end is connected to the roller. For satisfying the boundary condition at the rigid cylinder end, one can expand the deflections by applying assumed mode method as follows,

$$v(x(t),t) = \sum_{i=2}^{N} b_i(t) x(t)^i \quad (12)$$

where x^i is the mode shape which is dependent on time since the follower is driven by the cam to lengthen or shorten. $b_i(t)$ is the associated amplitudes for the transverse deflection. Though the polynomial expansion is a simple assumed mode method, it can easily formulate the moving boundary problem.

2.3 Hamilton's principle

Applying Hamilton's principle for the whole system, one has the variation equation

$$\int_{t_1}^{t_2} \delta(T_{rod} + T_{roller} - U_{rod} + \lambda_1\Phi_1 + \lambda_2\Phi_2)dt = 0 \quad (13)$$

where T_{rod} and T_{roller} are the kinetic energy of the follower rod and the roller, respectively. U_{rod} is the strain energy of the follower rod. $\lambda_1\Phi_1$ and $\lambda_2\Phi_2$ are the works done by the constraint forces.

Substituting equation (12) into Hamilton's principle (13), one can obtain the system equation of motion. The equation is expressed as

$$\mathbf{M}(\mathbf{Q})\ddot{\mathbf{Q}} + \mathbf{N}(\mathbf{Q},\dot{\mathbf{Q}}) + \boldsymbol{\Phi}_{\mathbf{Q}}^T\boldsymbol{\lambda} = \mathbf{0} \quad (14)$$

where $\mathbf{M}$, $\mathbf{N}$,and $\boldsymbol{\lambda}$ are mass matrix, nonlinear vector, and Lagrange multiplier, respectively. It is noted that the mass matrix is time-dependent. $\mathbf{Q}$ is the generalized coordinates vector and expressed as

$$\mathbf{Q} = [b_1 \quad b_2 \quad \cdots \quad b_N \quad x_E \quad \theta]. \quad (15)$$

The two constraints as expressed in equations (10) and (11) are combined as the following form

$$\boldsymbol{\Phi}(\mathbf{Q}) = [\Phi_1 \quad \Phi_2]^T = \mathbf{0} \quad (16)$$

Differentiating equation (16) with respect to time, one has the constraint velocity equation

$$\boldsymbol{\Phi}_{\mathbf{Q}}\dot{\mathbf{Q}} + \frac{\partial\Phi}{\partial t} = \mathbf{0} \quad (17)$$

Then differentiating equation (17) with respect to time, one has the constraint acceleration equation

$$\boldsymbol{\Phi}_{\mathbf{Q}}\ddot{\mathbf{Q}} = -(\boldsymbol{\Phi}_{\mathbf{Q}}\dot{\mathbf{Q}})_{\mathbf{Q}}\dot{\mathbf{Q}} - 2\frac{\partial\Phi_{\mathbf{Q}}}{\partial t}\dot{\mathbf{Q}} - \frac{\partial^2\Phi}{\partial t^2} \equiv \boldsymbol{\eta} \quad (18)$$

Combining the nonlinear ordinary differential equation (14) and the constraint acceleration equation (18), one obtains the following expression

$$\begin{bmatrix} \mathbf{M} & \boldsymbol{\Phi}_{\mathbf{Q}}^T \\ \boldsymbol{\Phi}_{\mathbf{Q}} & \mathbf{0} \end{bmatrix}\begin{bmatrix} \ddot{\mathbf{Q}} \\ \boldsymbol{\lambda} \end{bmatrix} = \begin{bmatrix} -\mathbf{N}(\mathbf{Q},\dot{\mathbf{Q}}) \\ \boldsymbol{\eta} \end{bmatrix} \quad (19)$$

The above equation is the differential-algebraic equation which governs the vibration of the translating roller-follower cam mechanism. Applying the Runge-Kutta integration method, one can obtain the vibration response of the follower.

Ⅲ. CAM PROFILES FOR RDFD MOTION

The schematic of a cam mechanism is shown in Fig. 1. The displacement function of the follower rod when the cam rotates an angle θ is denoted as $S(\theta)$. The rise-dwell-fall-dwell (RDFD) motion studied in this paper is described in Fig. 2.

Four cam profiles are considered with different rise and fall motions. They include the cycloidal displacement (sinusoidal acceleration) motion, the modified sinusoidal acceleration motion, the modified trapezoidal acceleration motion, and the 3-

4-5 polynomial motion. The displacement function $S(\theta)$ for the rise segment is given with the following five functions: (Chen [9])

1. Cycloidal displacement motion:

$$0 \le \theta \le \beta: \qquad S(\theta) = S_T\left(\frac{\theta}{\beta} - \frac{1}{2\pi}\sin(\frac{2\pi\theta}{\beta})\right) \tag{20}$$

2. Modified sinusoidal acceleration motion:

$$0 \le \theta \le \frac{\beta}{8}:$$

$$S(\theta) = S_T\left(\frac{\pi}{4+\pi}\frac{\theta}{\beta} - \frac{1}{4(4+\pi)}\sin(\frac{4\pi\theta}{\beta})\right) \tag{21.1}$$

$$\frac{\beta}{8} < \theta \le \frac{7\beta}{8}:$$

$$S(\theta) = S_T\left(\frac{2}{4+\pi} + \frac{\pi}{4+\pi}\frac{\theta}{\beta} - \frac{9}{4(4+\pi)}\cos(\frac{4\pi\theta}{3\beta} - \frac{\pi}{6})\right) \tag{21.2}$$

$$\frac{7\beta}{8} < \theta \le \beta:$$

$$S(\theta) = S_T\left(\frac{4}{4+\pi} + \frac{\pi}{4+\pi}\frac{\theta}{\beta} - \frac{1}{4(4+\pi)}\sin(\frac{4\pi\theta}{\beta})\right) \tag{21.3}$$

. Modified trapezoidal acceleration motion:

$$0 \le \theta \le \frac{\beta}{8}:$$

$$S(\theta) = S_T\left(0.38898\frac{\theta}{\beta} - 0.03095\sin(\frac{4\pi\theta}{\beta})\right) \tag{22.1}$$

$$\frac{\beta}{8} < \theta \le \frac{3\beta}{8}:$$

$$S(\theta) = S_T\left(2.44406\left(\frac{\theta}{\beta}\right)^2 - 0.22203\frac{\theta}{\beta} + 0.00723\right) \tag{22.2}$$

$$\frac{3\beta}{8} < \theta \le \frac{\beta}{2}:$$

$$S(\theta) = S_T\left(1.61102\frac{\theta}{\beta} - 0.03095\sin(\frac{4\pi\theta}{\beta} - \pi) - 0.30551\right) \tag{22.3}$$

$$\frac{\beta}{2} < \theta \le \frac{5\beta}{8}:$$

$$S(\theta) = S_T\left(1.61102\frac{\theta}{\beta} + 0.03095\sin(\frac{4\pi\theta}{\beta}) - 0.30551\right) \tag{22.4}$$

$$\frac{5\beta}{8} < \theta \le \frac{7\beta}{8}:$$

$$S(\theta) = S_T\left(-2.44406\left(\frac{\theta}{\beta}\right)^2 + 4.66609\frac{\theta}{\beta} - 1.22926\right) \tag{22.5}$$

$$\frac{7\beta}{8} < \theta \le \beta:$$

$$S(\theta) = S_T\left(0.61102 + 0.38898\frac{\theta}{\beta} + 0.03095\sin(\frac{4\pi\theta}{\beta} - \pi)\right) \tag{22.6}$$

4. 3-4-5 polynomial motion:

$$0 \le \theta \le \beta:$$

$$S(\theta) = S_T\left(10\left(\frac{\theta}{\beta}\right)^3 - 15\left(\frac{\theta}{\beta}\right)^4 + 6\left(\frac{\theta}{\beta}\right)^5\right) \tag{23}$$

In Eqs. (20) – (23), β is the period of the rise segment and S_T is the total lift magnitude. In this study, β is set to $\frac{\pi}{2}$. The above five motions are used for the rise portion of the cam. The rise functions are applicable to the fall with slight modification. To convert rise functions to fall functions, it is only necessary to subtract the rise displacement function $S(\theta)$ from the maximum lift S_T. The period of the fall segment is also set to $\frac{\pi}{2}$.

IV. NUMERICAL RESULTS AND DISCUSSIONS

The flexible follower vibration response of the translating cam with four different profiles for RDFD motion is investigated by using the numerical analysis. Due to the flexible follower, the contact point of the roller and the cam can not be determined by using kinematics analysis. The unknown contact point will be solved by using the proposed dynamic analysis including the geometric constraint equations. The transverse response at the end point of the follower is solved to show that the contact point is different from that under the assumption of the rigid follower rod. Four different cam profiles including the cycloidal displacement motion, the modified sinusoidal acceleration motion, the modified trapezoidal acceleration motion, and the 3-4-5 polynomial motion are employed to study the vibration of the flexible follower. The four different motions are applied to model the rise and fall displacement curves.

For the consistence of the comparison of the four different cam profiles, the related parameters are given the same values and listed in Table 1. The zero initial conditions are assumed. The time step for the numerical integration is set to $\frac{2\pi}{\Omega}\times 10^{-3}$ s.

The follower vibration with two rotation speeds of cam is analyzed. First, the rotation speed is set to $\Omega = 240$ rad/s. The time history of the transverse response at the end point of the follower undergoing the four different motions is obtained and plotted in Figs. 4-7. It is observed form the figures that the time response contains two major components for every period. Taking the first period to interpret, one can see that the response during $\Omega t = 0° \sim 90°$ and $180° \sim 270°$ has large amplitude with low frequency while that during $\Omega t = 90° \sim 180°$ and

$270° \sim 360°$ has small amplitude with high frequency. These may be explained that the large response amplitude during $\Omega t = 0° \sim 90°$ and $180° \sim 270°$ is excited since the follower undergoes the rise and the fall motions while the small response amplitude during $\Omega t = 90° \sim 180°$ and $270° \sim 360°$ is due to the dwell segments of the cam. The high frequency response during the dwell segments is the free vibration and may accord with the natural frequency of the flexible follower. This is verified by using the FFT analysis. From Figs 4-7, it is also shown that the high frequency response for the cycloidal displacement motion is the smallest and the low frequency responses are almost the same order for the different motions except for the modified trapezoidal acceleration motion. When the follower undergoes the modified trapezoidal acceleration motion, both the low and the high frequency responses are excited to the largest.

To gain an insight into the relationship of the response and the frequency, the fast Fourier transformation is performed to obtain the FFT spectra diagram for the four profiles. These spectra are shown in Figs. 8-11. The natural frequencies of the clamped follower rod for the two dwell segments are calculated. During $\Omega t = 90° \sim 180°$, the length of the follower from the bottom end of the rigid cylinder is 66 mm while that is 81 mm during $\Omega t = 270° \sim 360°$. The first three natural frequencies for the follower length, 66 mm, are 10469, 65615, and 183741 rad/s and for 81 mm are 6951, 43563, and 121990 rad/s. Except for the cycloidal displacement motion, there are many peaks appearing near the frequencies, 30Ω and 46Ω. They are close to the fundamental frequencies, 6951 and 10469 rad/s. That verifies the high frequency response is excited majorly due to the first natural mode. For low frequency peaks, it is found from Figs. 8-11 that the distinct peaks occur at even number times the rotation speed Ω. The largest peak occurs at four times Ω for all the different profiles. This may be explained that the cam profile experience four segments for every rotation thus the peak at four times Ω is excited most seriously. Furthermore, it is also observed from the figures that the peak at four times Ω for the cycloidal displacement motion is larger than that for the other three motions. The high frequency peaks for the modified trapezoidal acceleration motion are larger than those for the other three motions.

The cases with the rotation speed Ω=360 rad/s are also investigated. The FFT spectra diagrams are shown in Figs. 12-15. Many peaks are found near the frequencies, 19Ω and 30Ω. They are close to the fundamental frequencies, 6951 and 10469 rad/s. This phenomena is the same as the cases for Ω=240 rad/s. For low frequency peaks, the distinct peaks also occur at even number times Ω. The peak at four times Ω is also the largest one for all the different profiles. The peak at four times Ω for the cycloidal displacement motion is larger than that for the other three motions. The high frequency peaks for the modified trapezoidal acceleration motion are larger than those for the other three motions. Comparing the cases with Ω=240 rad/s and 360 rad/s from Figs 8-15, one can find that for all four profiles the responses with Ω=360 rad/s are larger than those with Ω=240 rad/s. This is due to the centrifugal force effect.

V. CONCLUSIONS

The flexible follower response of a translating cam with four different profiles for RDFD motion is studied. The governing equations are derived by using Hamilton's principle and the assumed mode method. Since the follower flexibility is considered, the contact point of the roller and the cam is an unknown. Two geometric constraints formulated to restrain the unknown position are substituted into the dynamics modeling with Lagrange multipliers. From the time histories of the follower response, it is obviously found that the response amplitude for the rise and the fall segments is larger while that for the dwell segments is smaller. The response for the modified trapezoidal acceleration motion is lager than that for the other motions. From the FFT spectra analysis, it is found that the high frequency response is excited majorly due to the first natural mode. The largest peak occurs at four times Ω for all the different profiles. The peak at four times Ω for the cycloidal displacement motion is larger than that for the other three motions. The high frequency peaks for the modified trapezoidal acceleration motion are larger than those for the other three motions.

ACKNOWLEDGEMENT

The authors are very thankful to the National Science Council of Taiwan for the grant NSC 98-2221-E-344-002 to carry out this project.

REFERENCES

[1]. Pasin, F., On dynamic stability of followers in cam mechanisms, Mechanism and Machine Theory, **18**(2), 1983, 151-155.

[2]. Yilmaz, Y., and Kocabas, H., The vibration of disc cam mechanism, Mechanism and Machine Theory, **30**(5), 1995, 695-703.

[3]. Felszeghy, S. F., Steady-state residual vibrations in high-speed, dewll-type, rotating disk cam-follower systems, Transactions of the ASME, Journal of Vibration and Acoustics, **127**, 2005, 12-17.

[4]. Teodorescu, M. and Rahnejat, H., Mathematical modelling of layered contact mechanics of cam–tappet conjunction, Applied Mathematically Modelling, **31**, 2007, 2610–2627.

[5]. Wu, L. I., Chang, W. T., and Liu, C. H., The design of varying-velocity translating cam mechanisms, Mechanism and Machine Theory, **42**, 2007, 352-364.

[6]. Cveticanin, L., Stability of motion of the cam–follower system, Mechanism and Machine Theory, **42**, 2007, 1238-1250.

[7]. Wu, L. I., Liu, C. H., Shu, K. L., and Chou, S. L., Disk cam mechanisms with a translating follower having symmetrical double rollers, Mechanism and Machine Theory, **44**, 2009, 2085-2097.

[8]. Naskar, T.K., and Acharyya, S., Measuring cam–follower performance, Mechanism and Machine Theory, **45**, 2010, 678-691.

[9]. Chen, F. Y., Mechanics and Design of Cam Mechanisms, Pergamon Press, New York, 1982.

Table I The related parameters values

S_T	15 mm	ρ	7.8×10^{-6} kg/mm^3
β	$\pi/2$	d	112 mm
γ_f	5 mm	γ_b	26 mm
A	78.54 mm^2	γ_r	5 mm
I	490.87 mm^4	m_r	0.003 kg
E	2.1×10^8 kg/mm · s^2	J_r	0.625 kg · mm^2

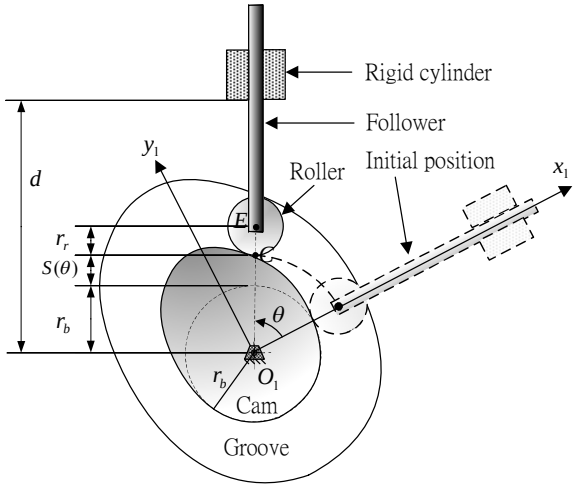

Fig. 1 Schematic of the cam mechanism.

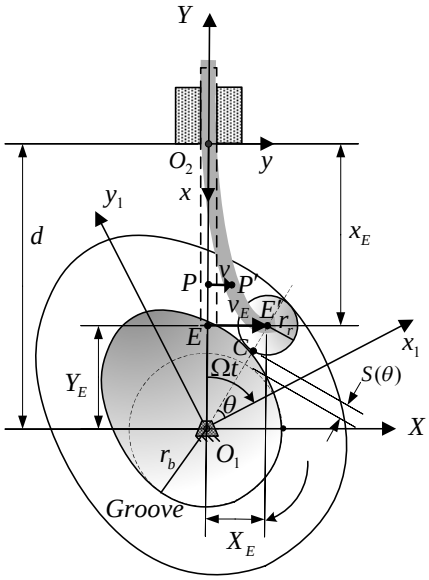

Fig. 2 Deformed configuration of the cam mechanism

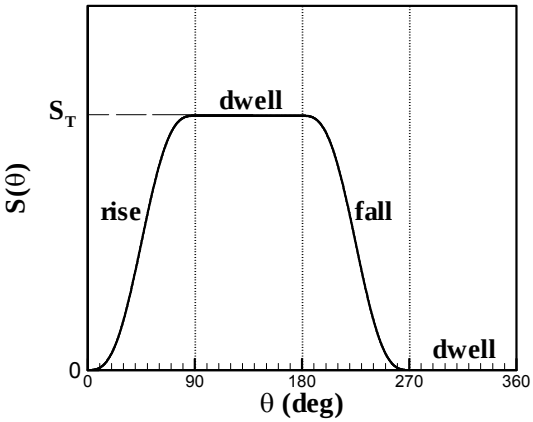

Fig. 3 The rise-dwell-fall-dwell motion of the follower.

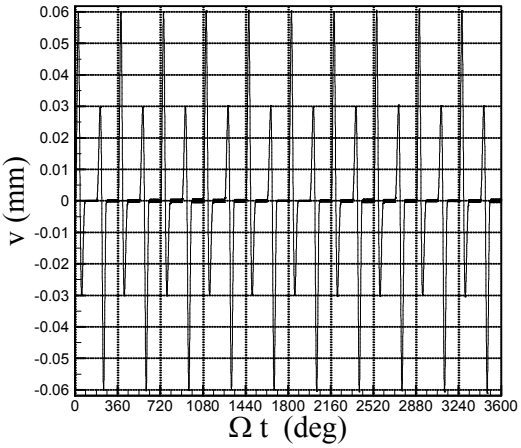

Fig. 4 The time history at the end point E of the follower undergoing cycloidal displacement motion for $\Omega = 240$ rad/s.

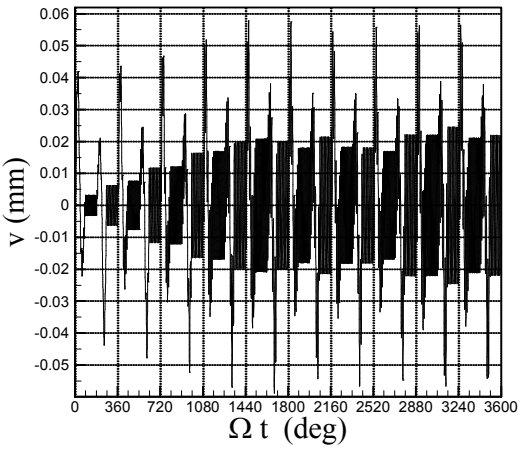

Fig. 5 The time history at the end point E of the follower undergoing modified sinusoidal acceleration motion for $\Omega = 240$ rad/s.

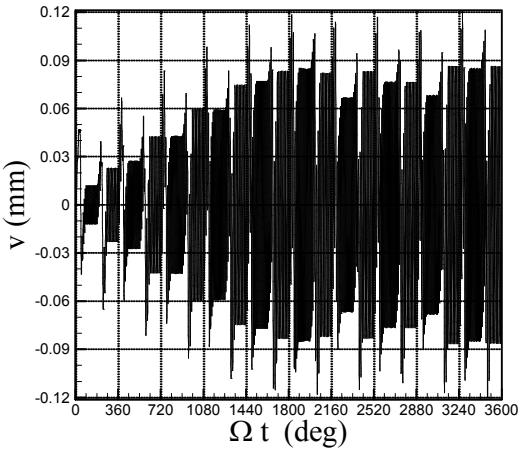

Fig. 6 The time history at the end point E of the follower undergoing modified trapezoidal acceleration motion for $\Omega = 240$ rad/s.

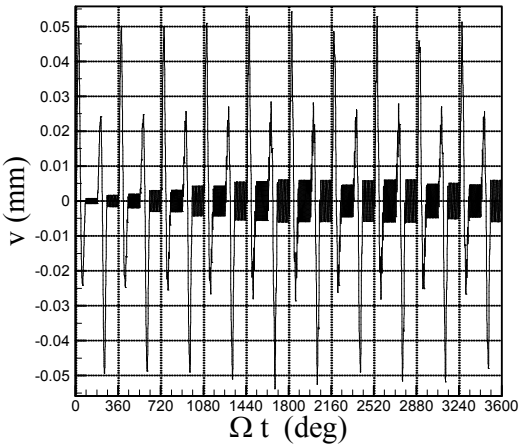

ig. 7 The time history at the end point E of the follower undergoing 3-4-5 polynomial motion for $\Omega = 240$ rad/s.

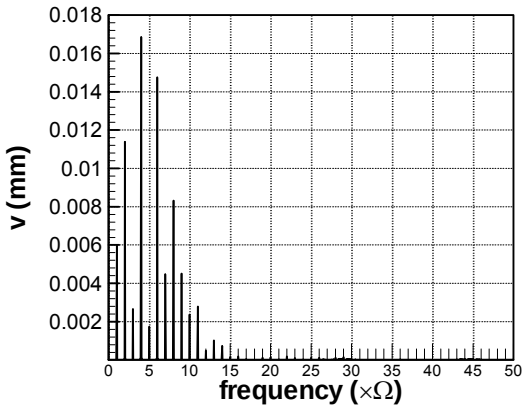

Fig. 8 The response spectra at the end point E of the follower undergoing cycloidal displacement motion for $\Omega = 240$ rad/s.

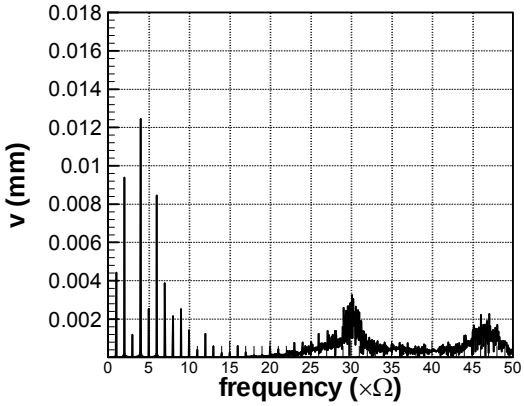

Fig. 9 The response spectra at the end point E of the follower undergoing modified sinusoidal acceleration motion for $\Omega = 240$ rad/s.

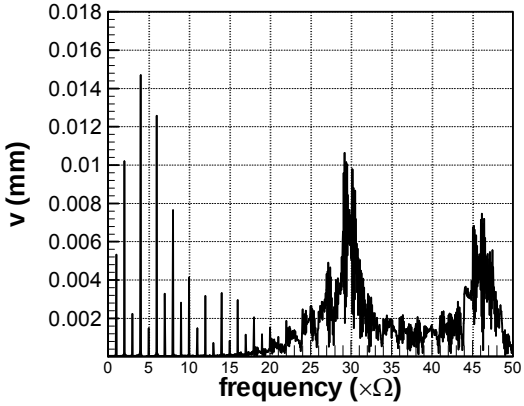

Fig. 10 The response spectra at the end point E of the follower undergoing modified trapezoidal acceleration motion for $\Omega = 240$ rad/s.

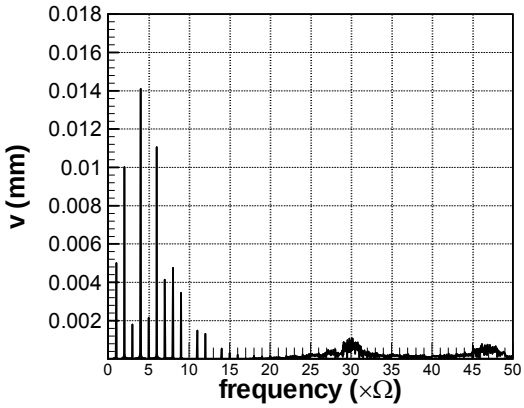

Fig. 11 The response spectra at the end point E of the follower undergoing 3-4-5 polynomial motion for $\Omega = 240$ rad/s.

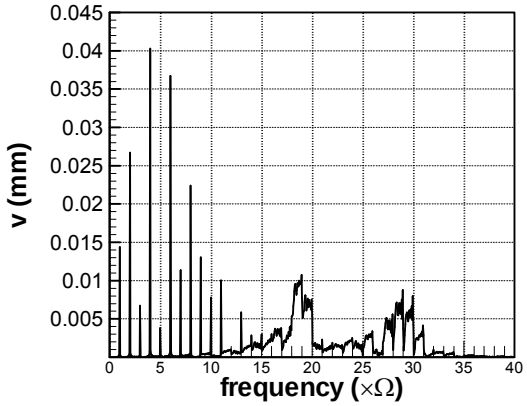

Fig. 12 The response spectra at the end point E of the follower undergoing cycloidal displacement motion for $\Omega = 360$ rad/s.

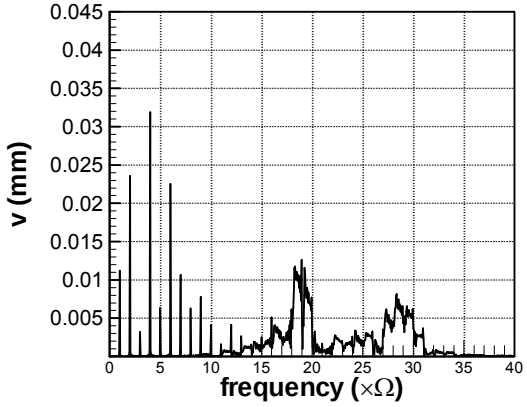

ig. 13 The response spectra at the end point E of the follower undergoing modified sinusoidal acceleration motion for $\Omega = 360$ rad/s.

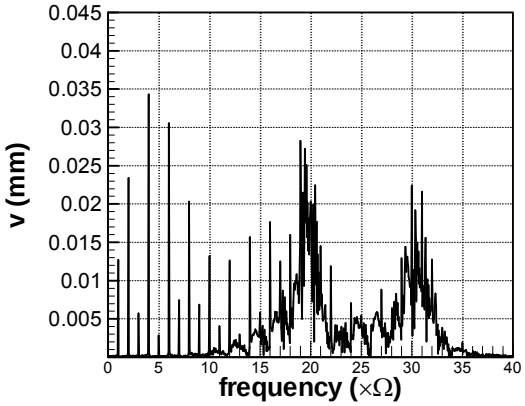

Fig. 14 The response spectra at the end point E of the follower undergoing modified trapezoidal acceleration motion for $\Omega = 360$ rad/s.

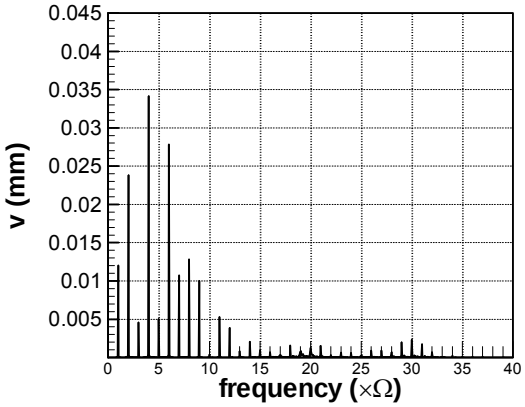

Fig. 15 The response spectra at the end point E of the follower undergoing 3-4-5 polynomial motion for $\Omega = 360$ rad/s.